



Depositional environment and sequence stratigraphy of the Upper Cretaceous successions in Eastern Alborz Basin, Damghan, Iran

Meysam Parimi ¹, Amin Navidtalab ^{2, *}, Mehran Ariyan ¹, Reza Aharipour ²

¹ Department of Geology, Science and Research Branch, Islamic Azad University, Tehran, Iran

² School of Earth Sciences, Damghan University, 36716-45667 Damghan, Iran

Received: 06 March 2023, Revised: 04 April 2023, Accepted: 11 April 2023

© University of Tehran

Abstract

A study on depositional environment, diagenetic history, and sequence stratigraphy of the upper Cretaceous successions of the boundary between the Central and Eastern Alborz zones is lacking. This study attempts to tackle this issue by analyzing a succession composed of 120 meters of medium- to thick-bedded limestones. Facies analysis led to the identification of facies associations of terrestrial, inner ramp (proximal, mid, and distal lagoon and shoal), mid ramp, outer ramp, and basin settings. According to the lateral and vertical changes in facies associations indicating gradual facies variations and the absence of large barrier reef organisms, a carbonate platform of ramp type with a bioclastic shoal is suggested for the studied succession. However, regarding the presence of turbidites in the transition of mid and outer ramp facies, a distally steepened ramp better suits the studied succession. Diagenetic study reveals products of eogenesis, mesogenesis, and telogenesis stages. Sequence stratigraphic analysis based on facies analysis and field observation denoted one 3rd-order depositional sequence, which its maximum flooding surface is equivalent to MFS K180 of the Arabian Plate (AP) with middle Maastrichtian age. A disconformity at the topmost of the studied succession correlates with the upper sequence boundary of megasequence AP9 around the Cretaceous–Paleogene boundary.

Keywords: Upper Cretaceous, Eastern Alborz, Depositional Environment, Sequence Stratigraphy, Carbonate Succession.

Introduction

Since the Cretaceous shares many similarities with the modern world, understanding of this part of the Earth's history could be significant for developing dynamic models of the globe (Haywood et al., 2019; Tierney et al., 2020). This understanding demands the reconstruction of critical data such as past depositional environments. Additionally, the Cretaceous was the time of tremendous global environmental changes on lands and in marines (Heimhofer et al., 2018; Leckie et al., 2002), of which, the latest cretaceous environmental transformations associated with Cretaceous/ Paleogene (KPg) boundary could be mentioned (Henehan et al., 2016, 2019; Hull et al., 2020; Linzmeier et al., 2020).

To reconstruct ancient sedimentary environments, carbonate sedimentary rocks can provide an important source of data (James & Jones, 2016). In the past sedimentary environments consisting of different sub-environments, incidents and events such as sedimentary conditions, sea-level changes, and diagenetic processes within sedimentary units that took place over time, have been recorded through deposited strata (Zarza & Tanner, 2010). These recorded changes could be unfolded by analyzing and examining these strata (Miall, 2010).

* Corresponding author e-mail: a.navidtalab@du.ac.ir

Despite the importance of the Cretaceous strata, some great basins have not been studied yet. Although many attempts have been made to study the Cretaceous successions of the Zagros Mountains, such studies in the Alborz chains are rare, especially in the transition of Central–Eastern Alborz. Most studies (e.g. Kalanat et al., 2015, 2016) have been conducted on the easternmost parts of the Eastern Alborz including Kopet Dagh.

In this study, a representative outcrop section of the upper Cretaceous successions was selected from the westernmost part of the Eastern Alborz Zone, located on the border between Eastern and Central Alborz zones, to define the depositional settings, diagenetic evolution, and sequence stratigraphy (Fig. 1A–B). Age assignment is according to the nannofossil biostratigraphy carried out in a neighboring section (Bodaghi et al., 2013) that its offset was implemented based on key stratigraphic units. It was applied and integrated with sequence stratigraphic interpretations to provide a more reliable stratigraphic framework for comparison with those in the Arabian Plate on the southeastern margin of the Neo-Tethys Ocean.

The study area, located on the northeastern margin of the Neo-Tethys (Fig. 1C), can represent the depositional characteristics of the border between the Western and Eastern Alborz zones. Although a study has analyzed the Cretaceous carbonate successions of this area in terms of carbonate nannofossils (Bodaghi et al., 2013), the lack of a study of depositional environment and sequence stratigraphy based on sedimentological data is evident. Therefore, this study aimed to evaluate facies changes, interpret the depositional environment, present a depositional model, and apply the results to determine and interpret sedimentary sequences.

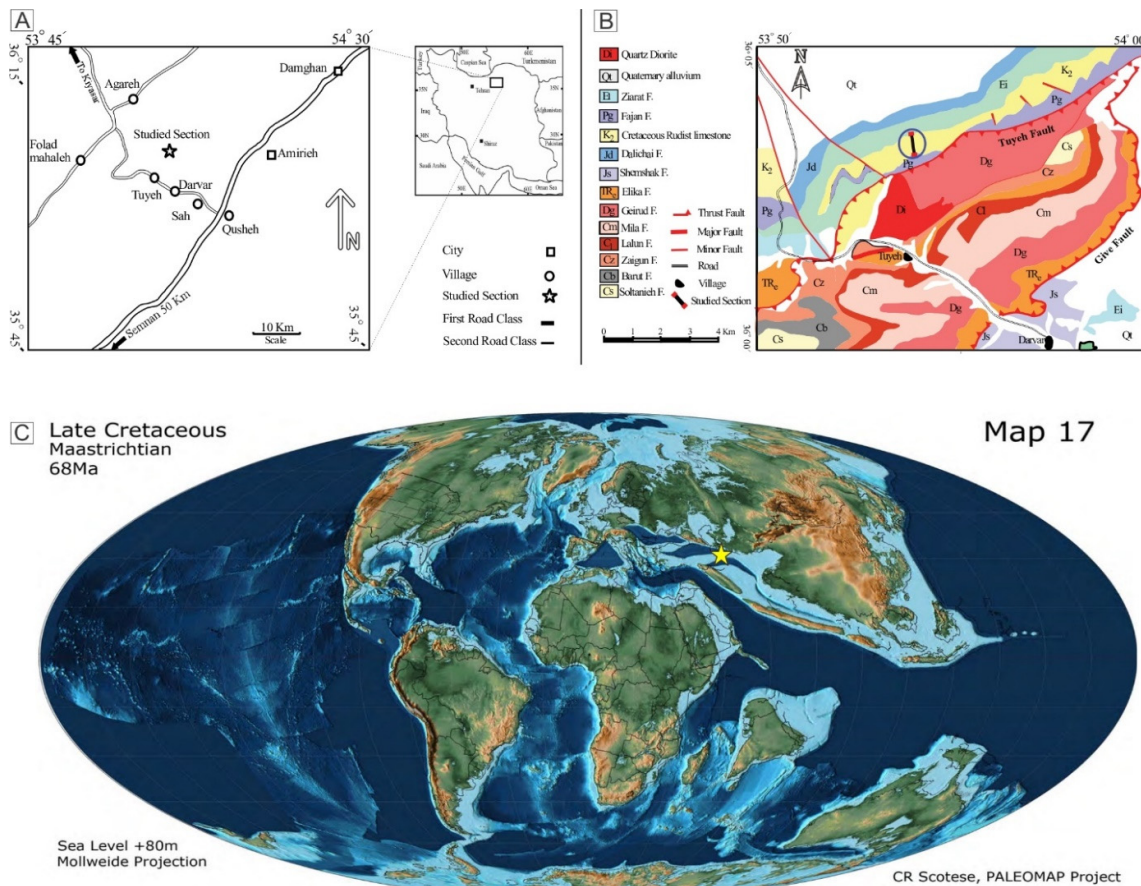


Figure 1. A. Geographical location and access road to the study area; B. Geological map of the study area derived from the 1:100000 geological map of Kiasar; C. Paleogeographic reconstruction of the Late Cretaceous (Maastrichtian; 68 Ma). The study area is shown by yellow star

Geological Setting and Stratigraphy

The Alborz Mountains are part of the Alpine–Himalayan Orogenic Belt in Western Asia. These mountains are bordered by the Caspian subducted block to the north and by the Central Iranian blocks to the south (Berberian, 1976). According to the geological and structural investigations by Stocklin (1974), the Alborz Mountains are structurally subdivided into three regions, from west to east, including (1) the Western Alborz zone which continues from Qazvin to the west of Iran, and encompasses Azarbaijan Mountains; (2) the Central Alborz zone which extends from Qazvin to Semnan; (3) the Eastern Alborz zone that ranges from the Semnan fault to the northern areas of Mashhad, and its continuation joins the western Hindu Kush in Afghanistan. The study area is located in the westernmost of the latter.

Subduction initiation (Moghadam et al., 2020; Moghadam & Stern, 2021), Neo-Tethys closure (Navidtalab et al., 2016, 2020), ophiolite obduction (Alavi, 2004, 2007), basement block reactivation (Mehrabi et al., 2015), active salt tectonic (Piryaei et al., 2010; Piryaei et al., 2011), and vast magmatism unanimously indicate a very active tectonism in Iran during the Cretaceous. The Upper Cretaceous successions demonstrate very variable depositional facies characteristics. Seemingly, unlike the Lower Cretaceous, sedimentary basins of the Upper Cretaceous in Iran have been detached, and each basin was governed by individual conditions. In this sense, the Upper Cretaceous successions of Iran, except for Zagros and Kepet Dagh, have not been formally named, and have local names instead. One of the characteristics of the Late Cretaceous of Iran is the repetition of tectonic movements related to events comparable to the Subhercynian cycle. This justifies the frequent sedimentary hiatuses and erosional surfaces within these upper Cretaceous successions (Aghanabati, 2006).

The studied succession is composed mostly of cliff-forming massive rudistic limestones at the lower part which is known as K_2^{ll} . It bears rare intercalations of marls near its top. The upper part of the succession is made of medium- to thin-bedded limestones and marl and marlstones intervals at the top which could be considered as K_2^{ml} . Both K_2^{ll} and K_2^{ml} are of Upper Cretaceous (Jalilian et al., 1992).

The basal rudistic succession was not studied due to the hard access, and is overlain by Fajan Formation, with an erosional boundary in between. The section can be lithologically subdivided into two units, with the lower unit composed of thick-layered to massive rudistic limestones, and the upper unit is made of shales, marls, and limestone. The section under study is located 60 km southwest of Damghan (Figure 1), and this section with an Upper Cretaceous age is shown on the 1/100,000 Kiasar geological map (Fig. 1B).

The Upper Cretaceous strata in Eastern Alborz have been studied for their biostratigraphy based on calcareous nannofossil in four sections including Mojen (Bodaghi & Hadavi, 2015), Namazgah and Shahdar (Bodaghi & Hadavi, 2014), and Cheshmeh Gholghol (Bodaghi et al., 2013). The latter is located in the vicinity of the here-presented section, and represents a calcareous nannofossil assemblage of 51 species assigned to 23 genera. They indicate CC16 to CC26 nannofossil biozones of Late Santonian to Late Maastrichtian age (Bodaghi et al., 2013). Paleocological reconstructions prove that the Upper Cretaceous successions of interest were deposited under warm paleoclimatic conditions throughout lower latitudes, and in shallow depositional environments (Bodaghi et al., 2013).

Materials and methods

The studied Tuye-Darvar outcrop section is located 60 km southwest of Damghan (Figure 1), at the southeastern flank of the Kuh-e-Sorkh syncline ($36^{\circ} 02' 16''$ N; $53^{\circ} 50' 36''$ E), in the vicinity of the Dade Hasan spring, between Darvar and Tuye villages. There, a stratigraphic succession covering 120 m of the Cretaceous sediments was described and sampled. In total, 126 samples

were collected at an average spacing of 95 cm, although in some cases spacing exceeds 1.5 m. The here applied working approach includes sedimentology and diagenesis studies based on field observations and thin-section petrography. Facies recognition is based on the integration of sedimentological and paleontological (macrofossils) field observations with thin-section analysis. For the classification of limestones, the scheme of Dunham (1962) modified by (Embry & Klovan, 1971) was applied. To determine microfacies associations and depositional environment, the standard microfacies assemblages suggested by (Flügel, 2010) were considered.

Results

Field observations and lithostratigraphy

The studied section is composed of five main units including (Fig. 2A): (1) Massive rudistic limestone (SN1-2) with large rudist shells (Fig. 2B), which at its top, a thick limestone layer occurs with abundant, but smaller rudist shells perpendicular to the bed plane (SN3; Fig. 2C); (2) medium- to thick-bedded limestones with thin intercalation of easily-weathered marlstones as shallowing-upward cycles (Fig. 2A and D), which towards the top of this unit, the marlstone horizons disappear (samples 18-36), and bioturbation is observed (Fig. 2E). Again, from this part of the unit (SN36), marlstone-limestone cycles retrieve. In limestones (SN47-49), bioturbation become abundant again (Fig. 2F), and limestones show a calcareous sandy nature; (3) From SN50, the clay-sized argillaceous content of the strata increases to show a nearly thick interval of highly weathered marlstones (Unit 3 in Fig. 2A); (4) Above the marlstone unit, lithology changes to medium- to very thick-bedded limestones containing abundant, well-preserved, whole-body rudists, indicating rudist boundstone similar to the top of unit 1 (Unit 4 in Fig. 2A); (5) terrigenous materials including sand- to cobble-sized grains dominate the top of the section (Fig. 2G). This lithology shows the transition between marine and terrestrial settings that starts with sandstones. The color is red in this interval which may bear testimony to the continental dominance. This unit could be ascribed to the Fajan Formation (Fig. 2A).

Depositional facies and facies associations

The aim of facies identification is to investigate changes in the environment such as paleoclimate, water energy, and changes in the relative sea level (Bachmann & Hirsch, 2006). Here, a detailed study of the Cretaceous depositional strata based on lithology, sedimentary features, texture, and fossil content led to the identification of clastic petrofacies and carbonate microfacies (Figs. 3–5) which belong to eight facies associations as follows (Table 1).

Terrestrial facies group

Conglomerate petrofacies

This facies is composed of considerable terrigenous content such as coarse-grained (granule to pebble) quartz and lithic grains (Fig. 3A). Limestone lithics are the most frequent grains, nonetheless, cherts are frequently seen. The limestone lithic grains are composed of abundant spicules which may be of Lar Formation origin of Jurassic age. The matrix is mainly micritic lime, which are sparsely replaced by cements.

Sandstone petrofacies

The essential constituents of this facies include limestone and chert lithics in accompaniment with quartz grains (Fig. 3B).

Table 1. Main characteristics of the identified facies and facies groups in the Upper Cretaceous succession in the studied section

Facies code	Facies Name	Lithology	Allochems (skeletal & non-skeletal)	Structures and features	Facies Group	Setting
MF1	Conglomerate petrofacies	Siliciclastic	Carbonate lithics, chert, quartz	Cross bedding	FG1	Terrestrial
MF2	Sandstone petrofacies	Siliciclastic	Carbonate lithics, chert, quartz	Lamination, cross bedding	FG2	Terrestrial
MF3	Sandy peloid wackestone	Limestone	Pellet, peloid, quartz	-	FG3	Inner ramp (proximal lagoon)
MF4	Benthic foraminifera peloid pellet, rudist debris, gastropod pack/grainstone	Limestone	Benthic foraminifera, peloid, pellet, intraclast, rudist fragments, red algae, gastropod, quartz, chert	-	FG4	Inner ramp (mid lagoon)
MF5	Benthic foraminifera, peloid, pellet, rudist wacke to grainstone to floatstone and boundstone	Limestone	Benthic foraminifera, small to large rudist fragments, stabilized aragonitic bivalves, red algae, peloid, pellet	-	FG5	Inner ramp (distal lagoon)
MF6	Peloid, benthic foraminifera, bioclast wackestone to grainstone	Limestone	Peloid, benthic and planktic foraminifera, red and green algae, bioclast, echinoderm, stabilized aragonitic bivalves, sparse rudist debris, quartz	Rounded and well-sorted grains	FG6	Inner ramp (barrier shoal)
MF7	Intraclast, peloid, bioclast, benthic and planktic foraminifera wacke to packstone	Limestone, dolomitic limestone, dolomite	Intraclast, peloid, bioclast, benthic and planktic foraminifera, sparse green algae, echinoderms, small and rare rudist debris, and thin shelled bivalve, silt-sized quartz	Simultaneous occurrence of planktic and benthic foraminifera	FG7	Mid ramp
MF8	Bioturbated foraminifera, spicule, radiolarian, mudstone	Limestone, dolomitic limestone, dolomite	Sponge spicule, benthic and planktic foraminifera, radiolaria, winnowed quartz	Bioturbation, Grain grading	FG8	Outer ramp
MF9	Silty/sandy, intraclast, bioclast wackestone (calciturbidite)	Limestone, dolomitic limestone, dolomite	Intraclast, bioclast, sponge spicule, benthic and planktic foraminifera, radiolaria, winnowed quartz	Grain grading	FG8	Outer ramp
MF10	Spicule, radiolarian, peloid mud to packstone	Limestone, dolomitic limestone, dolomite	Radiolaria, sponge spicule, peloid, winnowed quartz	Bioturbation	FG9	Basin

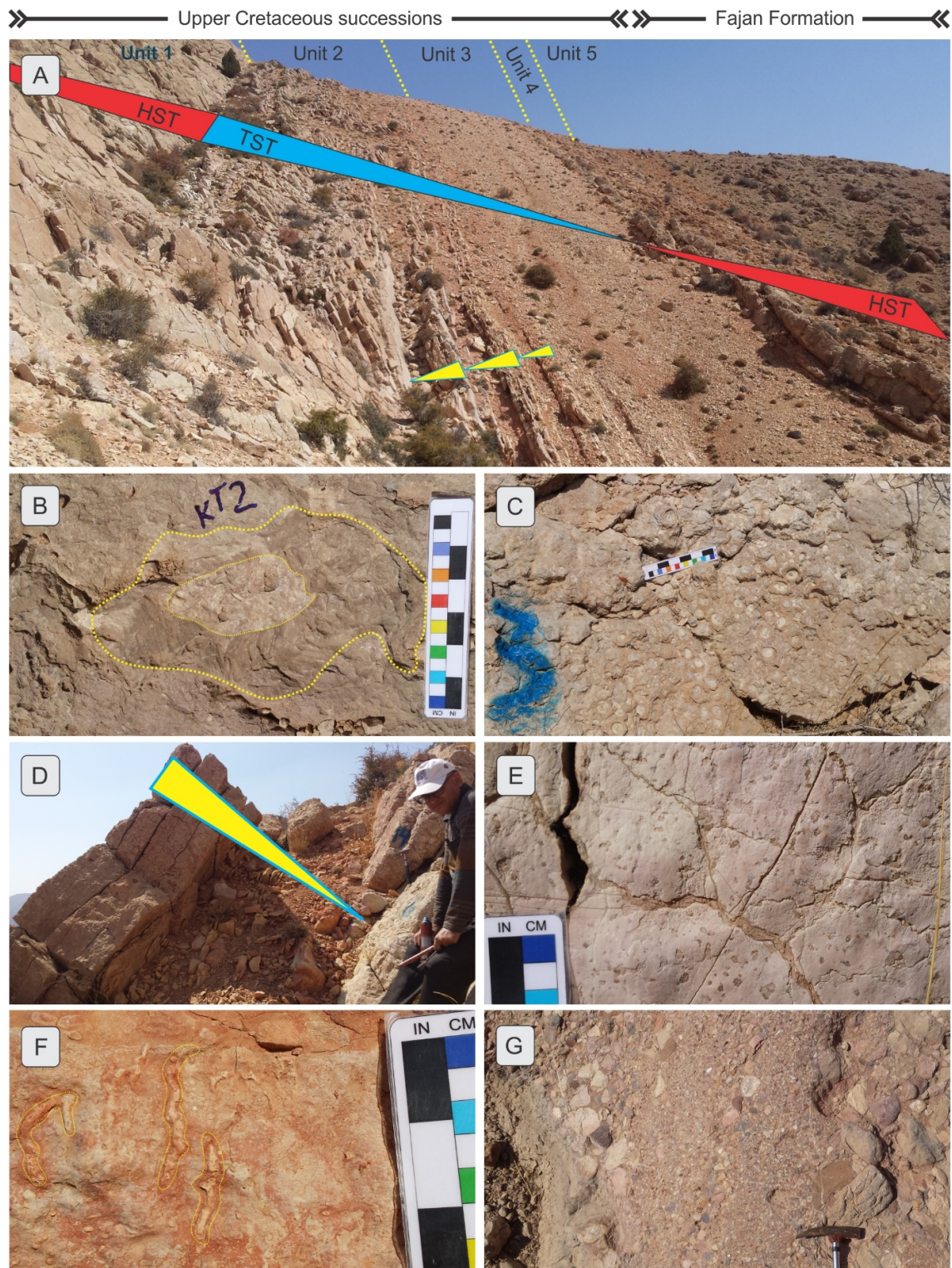


Figure 2. Field photographs of the studied section: A. the studied section of the Upper Cretaceous successions showing sequence stratigraphic elements, overlain by the conglomeratic Fajan Formation. Yellow triangles show some shallowing upward cycles; B. Massive limestones of Unit 1 containing large-sized rudist shells; C. Thick-bedded rudist boundstone at the top of Unit 1; D. Couplets of marlstone-limestone showing shallowing upward cycles; E-F. Abundant bioturbation in limestones; G. Sandstones and conglomerates of the transition between the Upper Cretaceous successions and the Fajan Formation

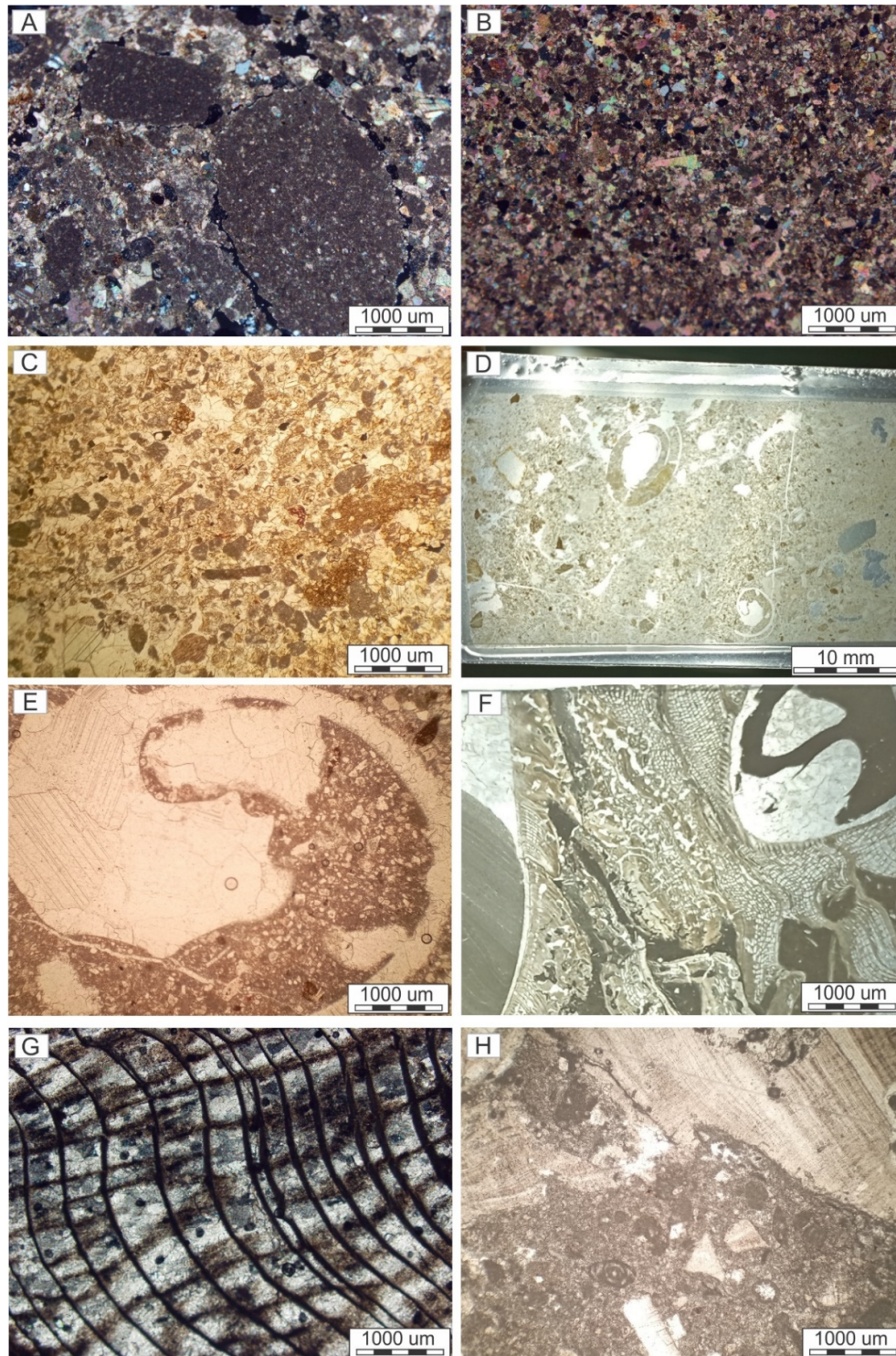


Figure 3. The microfacies identified in the studied thin-sections: A. Conglomerate with carbonate lithics; B. Fine sized Sandstone; C. Sandy Pellet Peloid Wacke/packstone; D–E. Pellet Gastropod Packstone; F–G. Rudist Boundstone; H. Rudist Rudstone facies

Non-skeletal calcareous components such as peloids and skeletal fragment such as echinoderms are rarely observed. The grain size ranges between medium to coarse sand, but with some granule sized grains. The matrix is mainly lime which in rare cases are replaced by calcite cements.

Environmental interpretation: the abundance of quartz and chert grains, and the mixing of these particles with some rare skeletal fragments and their predominantly red color ascribes this petrofacies to the terrestrial which sometimes was affected by marine processes. These petrofacies are observed on the top of the studied section, and are attributed to the Fajan conglomeratic Formation. They show the transition from marine to terrestrial environment at the time of deposition.

Inner ramp facies group

Proximal lagoon

It includes Sandy Pellet Peloid Wackestone containing considerable angular quartz grains (Fig. 3C). The quartz grains are silt to medium sand sized and compose more than 45% of the facies. After conglomerates, this facies contains the highest amount of terrigenous content. Abundant terrigenous content shows the proximity of this facies to the terrestrial setting, and the input of quartz grains during the deposition of this facies.

Mid lagoon

Facies of this sub-setting include Benthic Foraminifera Peloid Pellet Pack/Grainstone, Benthic Foraminifera Peloid Pellet Rudist debris Pack/Grainstone, and Pellet Gastropod Packstone (Fig. 3D–E). The two former facies contain benthic foraminifera, peloid, sparse intraclasts, and sparse, small to large sized rudist debris. Pellet and red algae are other components of these facies. Rare and sparse silt sized angular quartz, and sometimes cherts, are the terrigenous content. Pellet Gastropod Packstone consists of large gastropods along with pellets, peloid, and benthic foraminifera. Terrigenous grains mostly include sand to granule sized quartz, chert, and limestone lithics.

Distal lagoon

Benthic Foraminifera Peloid Pellet Rudist Pack/Grainstone, Rudist Floatstone, Rudist Boundstone (Fig. 2C and 3F–H), and Rudist Wackestone facies are the most important facies of this sub-setting. The difference between the former facies and similar facies of proximal lagoon is the abundance and larger rudist debris. Rudist Boundstone and associated wackestone and rudstone facies are the most prominent facies of the distal lagoon. In the field, the rudists are perpendicular to the bed plane, so it seems more appropriate to consider them as boundstone facies. Other components include benthic foraminifera, red algae, scattered aragonitic bivalves and gastropods, peloids, and pellets. Most of the subordinate components are as fillings in pores of rudist shells. Rudistic facies, mainly boundstones, are observed at the top and base of the section.

Barrier shoal

Peloid Grain/Packstone, Peloid Benthic Foraminifera Pack/Grainstone, Bioclast Grainstone, Foraminifera Peloid Pack/Grainstone, and Bioclast Foraminifera Wackestone are the most frequent facies of this setting. The skeletal fragments of the facies include mostly benthic foraminifera, echinoderm, bivalves, red algae, sparse rudist debris, and in rare cases, planktic foraminifera and green algae. Peloid is the main non-skeletal component of these facies (Fig. 4A). Micritization of allochems is frequent. The grains are mostly rounded, showing high energy environment with continuous movements. Dissolution and cementation are pervasively

observed in these facies. Very fine, angular, silt sized, quartz grains are also sparsely distributed in these facies.

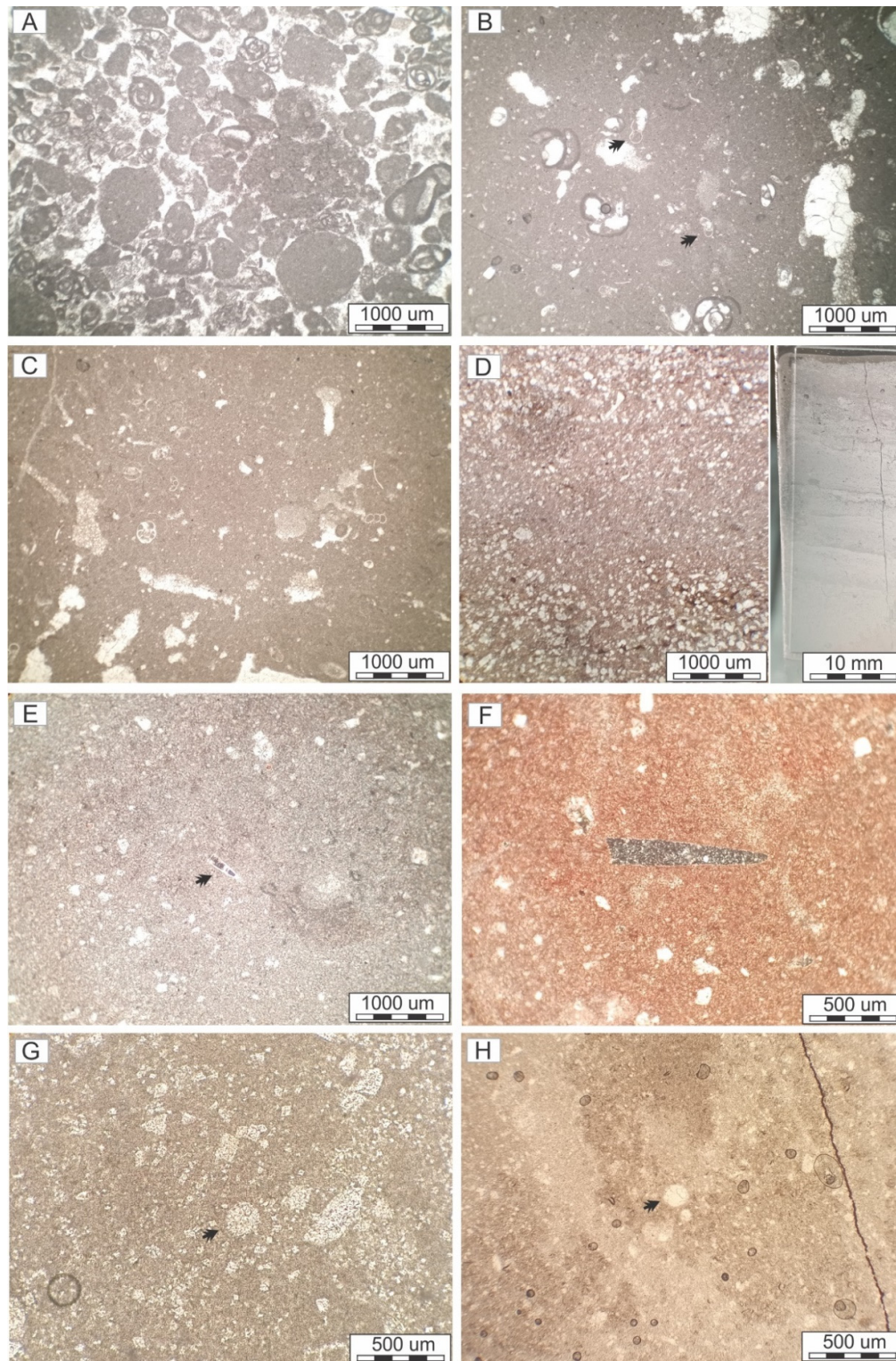


Figure 4. photomicrographs of different facies: A. Peloid Benthic Foraminifera Pack/Grainstone; B. Bioclast Foraminifera (benthic and planktic) Wacke/packstone; C. Planktic Foraminifera Mudstone; D. Spicule Silty/Sandy Mudstone (graded turbidities); E–F. Spicule Mudstone showing siliceous spicule with central canal, G. Radiolarian Mudstone, H. Bioturbated Radiolarian Mudstone

Environmental interpretation: The described microfacies are mostly attributed to the inner-ramp setting (Tucker, 2001; van Buchem et al., 2006; Flügel, 2010; Enayati-Bidgoli & Navidtalab, 2020). The co-occurrence of organisms such as red algae, gastropods, and rudists along with pellets shows restricted waters with higher salinity of lagoonal setting for these facies. Lagoon facies are typically placed between the terrestrial petrofacies and the barrier facies in a vertical sedimentary sequence (Lasemi, 2012). This facies group includes carbonate facies formed in different parts of the lagoon which is divided into the proximal, mid, and distal lagoon (van Buchem et al., 2006). The abundance of benthic foraminifera (such as miliolids), gastropod, and micrite (wackestone and mudstone facies) indicate the relatively low energy conditions and depositional environment of the lagoon (Bebout et al., 1981). Packstone and grainstone facies are also formed in more energetic conditions, such as the back-shoal setting located in lagoon.

Rudist bioherms are mostly found in distal lagoon as small buildups which also produce debris to form rudist debris facies of reef talus (Steuber, 1994, 2000, 2002). Reefs are often placed between units with different lithological characteristics and are thicker than carbonates of the same age (Feiznia, 1998). However, the studied rudist boundstones form medium- to very thick-layered horizons.

Mid ramp facies group

Bioclast Intraclast Wacke/Packstone, Bioclast Foraminifera Wacke/packstone, and Peloid Foraminifera Wacke/packstone (Fig. 4B) are the main microfacies. The most characteristic feature of these facies is the simultaneous occurrence of planktic and benthic foraminifera. The variable factor in these facies group is the frequency of planktic versus benthic foraminifera. Other components include rare to abundant peloid, sparse green algae, echinoderms, small and rare rudist debris, and thin shelled bivalve. The terrigenous components enclose angular, fine, silt sized quartz with variable abundances. However, its abundance barely exceed 10%.

Environmental interpretation: co-occurrence of open marine fauna such as planktic foraminifera, green algae, and echinoderms show nearly well circulated marine waters which mostly show the mid ramp setting (Flügel, 2010). Winnowed silts also corroborates the distance from marginal setting such as inner ramp.

Outer ramp facies group

Bioturbated Foraminifera Radiolarian Mudstone, Radiolarian Foraminifera Mudstone, Planktic Foraminifera Mudstone (Fig. 4C), Intraclast Bioclast Wackestone (calciturbidite), Bioturbated Mudstone, Silty Bioturbated Mudstone, Spicule Bioturbated Mudstone, and Spicule Silty/Sandy Mudstone (graded turbidities; Fig. 4D–F) are the microfacies distinguished for outer ramp in the studied section. Facies of this setting are mostly mudstones. Radiolarians are very rare. Spicules are also sparsely distributed, but they are more common than radiolarians. Winnowed, angular fine silt to fine sand sized quartz grains are commonly observed, especially in turbidities. Turbidities are very well graded.

Environmental interpretation: Turbidities are always observed between mid ramp and outer ramp facies in the studied section and indicate a probable break in the platform. They are considered as the end of mid ramp or onset of outer ramp settings in distally steepened ramp models (Flügel, 2010). Pervasive bioturbation in the mudstone facies of this setting may indicate low sedimentation rates due to a deeper setting and distance from the platform margin. The presence of sponge spicules and radiolarians as the main allochems also corroborate the deeper nature of these facies.

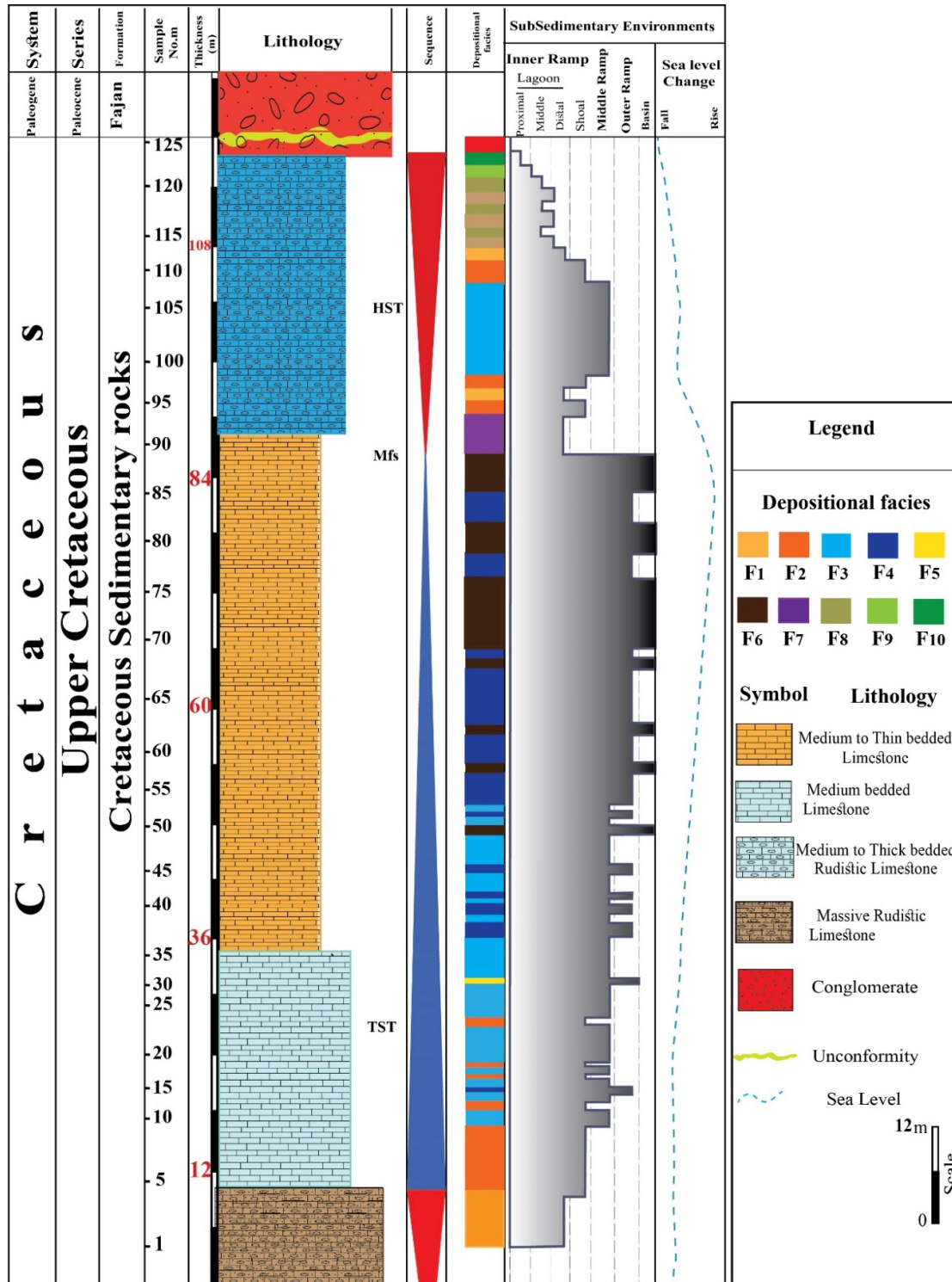


Figure 1. Stratigraphic column, microfacies distribution, sedimentary settings, relative sea level changes and sequence stratigraphy of the studied section

Basin facies group

Radiolarian Peloid Packstone, Radiolarian Bioturbated Mudstone (Fig. 4G–H), Spicule Bioturbated Radiolarian Mudstone, and Radiolarian Spicule Mudstone compose the basin

setting. The most important feature is the privilege of radiolarians. Although they are not abundant, they appear as the most important allochems in these facies. Winnowed, angular, fine, silt sized quartz is observed occasionally. In some samples, bioturbation is pervasive. Another component that could be found in some limited samples is peloid.

Environmental interpretation: Among the observed allochems in the studied samples, radiolarians are from the deepest setting (van Buchem et al., 2006). However, the rarity of these fauna in the samples may be related to the either lacking nutrients or input of winnowed silt-sized quartz and other terrigenous materials. Nonetheless, facies containing these fauna belong to the deepest setting which could be proved by field observation and co-occurrence of outer and mid ramp facies. These facies are observed in the middle to near top of the section where bioturbated medium- to thin-layered strata are interbedded with thin marls (unit 3 in Fig. 2).

Diagenesis

Diagenesis includes physical and chemical processes that modify the characteristics of sediments during deposition and after deposition (Morad et al., 2013). Diagenesis can cause the loss of primary sedimentary features, but can leave valuable information about the history of the post-depositional environment, pore water composition and temperature, and the tectonic evolution of an area (Scholle & Scholle, 2006). Climate, tectonics, sea-level changes, topography, hydrology, the primary composition of sediments, grain size, type of interparticle fluids, temperature, and pressure are the most important controlling factors of diagenesis (Miller et al., 2012; Nascimento et al., 2019; Wu et al., 2019; Baques et al., 2020). The most important diagenetic processes that were identified in the studied sequences are as follows:

Micritization:

In some thin-sections, micritization around skeletal grains is well developed (Fig. 6A). This process occurs in the early stages of diagenesis, simultaneous with the sedimentation of particles and under conditions of slow sedimentation rate (Khalifa et al., 2014; Gharechelou et al., 2020), and is characteristic of marine diagenetic environments (Sahraeyan et al., 2013).

Bioturbation

This process has been observed in some thin-sections, however, in the field, it is pervasive in some intervals (Fig. 2E–F; Fig. 4H; Fig. 6B). Bioturbation and excavation present the biological and depositional conditions as valuable indicators of simultaneous changes with sedimentation and diagenesis. Bioturbation occur pervasively in settings where oxygen and feeding are sufficient in the existing interparticle spaces, and the sedimentation rate is low.

Cementation

Blocky cement

This cement filled the open space between the grains and the cavities in the studied deposits with coarse crystals (Fig. 6C). This type is usually found in meteoric diagenesis environments (vadose or phreatic), burial environments, and rarely in marine reefs and hardgrounds (Flügel, 2010). It is considered as second- and third-generation cement, and its expansion indicates the low ratio of Mg/Ca in their constituent fluids (Purser, 1978).

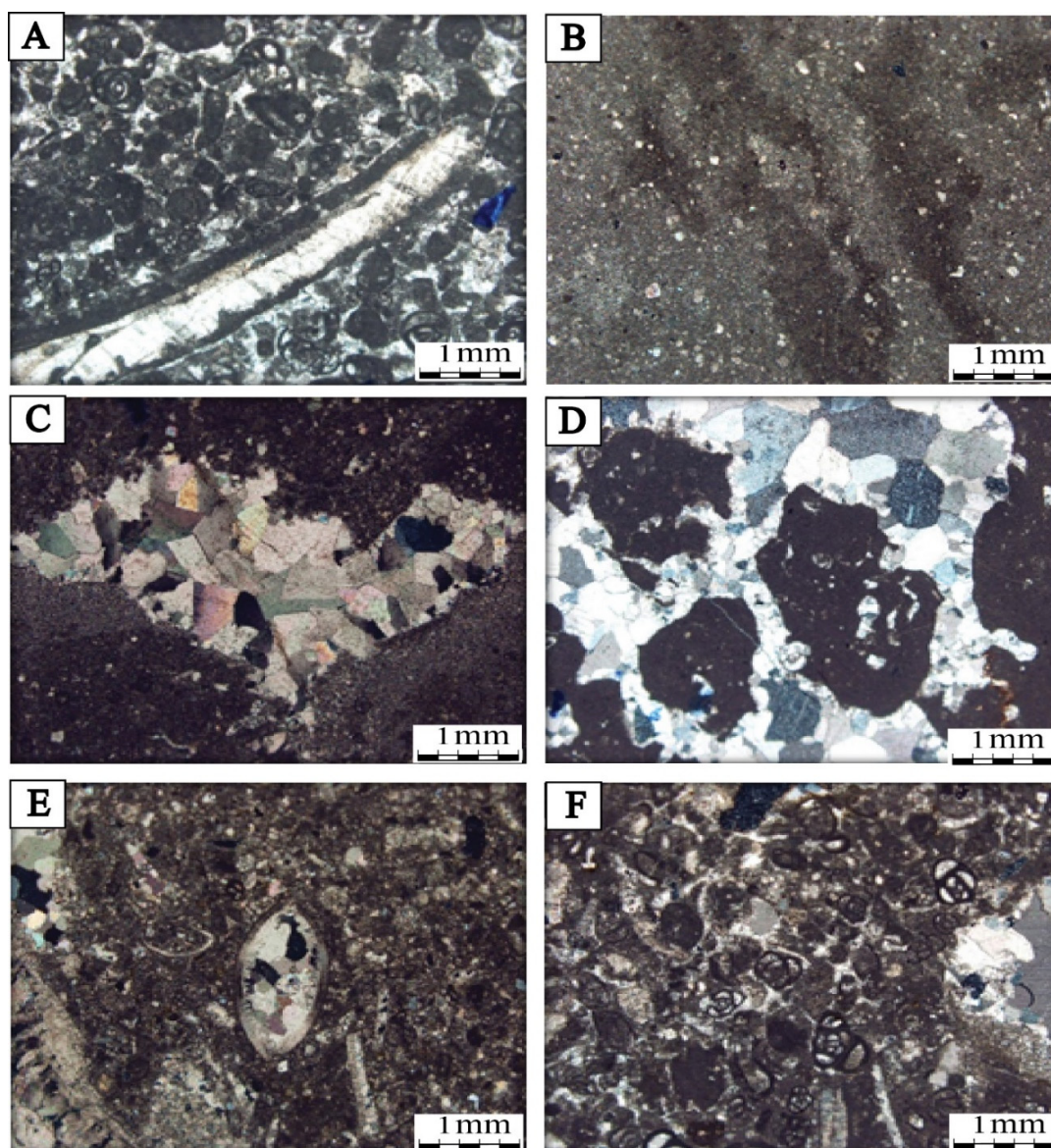


Figure 2. Diagenetic processes identified in the studied section: A. Micritization; B. Bioturbation; C. Blocky cement; D. Equant cement; E. Drusy cement; F. Physical compaction

Equant cement

In the studied samples, this cement is observed as filling in the space between allochems and fractures (Fig. 6D). This type of cement is more abundant than other cement types, and is usually formed in meteoric diagenesis (Okubo et al., 2015).

Drusy cement

This cement is the most frequent type identified in the studied samples, filling most cavities (Fig. 6E). It is formed as cavity filling in the interparticle space and within the skeletal pores, in mold cavities resulting from dissolution, and along the fractures, with the crystal characteristics of equidimensional to elongated, and euhedral to subhedral crystals (Flügel, 2010).

Compaction

Both physical and chemical compactions are observed in the studied samples. Physical compaction usually begins after deposition and causes compaction of sediments (Fig. 6F), loss of interparticle water, tighter grain arrangement, and reduced porosity (Ehrenberg et al., 2002). Chemical compression is also visible in dissolution veins and various stylolites in many facies (Fig. 7A), and also in the field (Fig. 2E). Chemical compaction may be the source of calcium carbonate for the formation of burial cements (Okazaki et al., 2014).

Geopetal fabric

In the studied thin-sections, geopetal fabric was mostly seen inside gastropod shells (Fig. 7B). Geopetal fabric is a good indicator for determining the layers top. These structures record the horizontal surface at the deposition time and, in some cases, show the initial slope (Tucker & Wright, 1990).

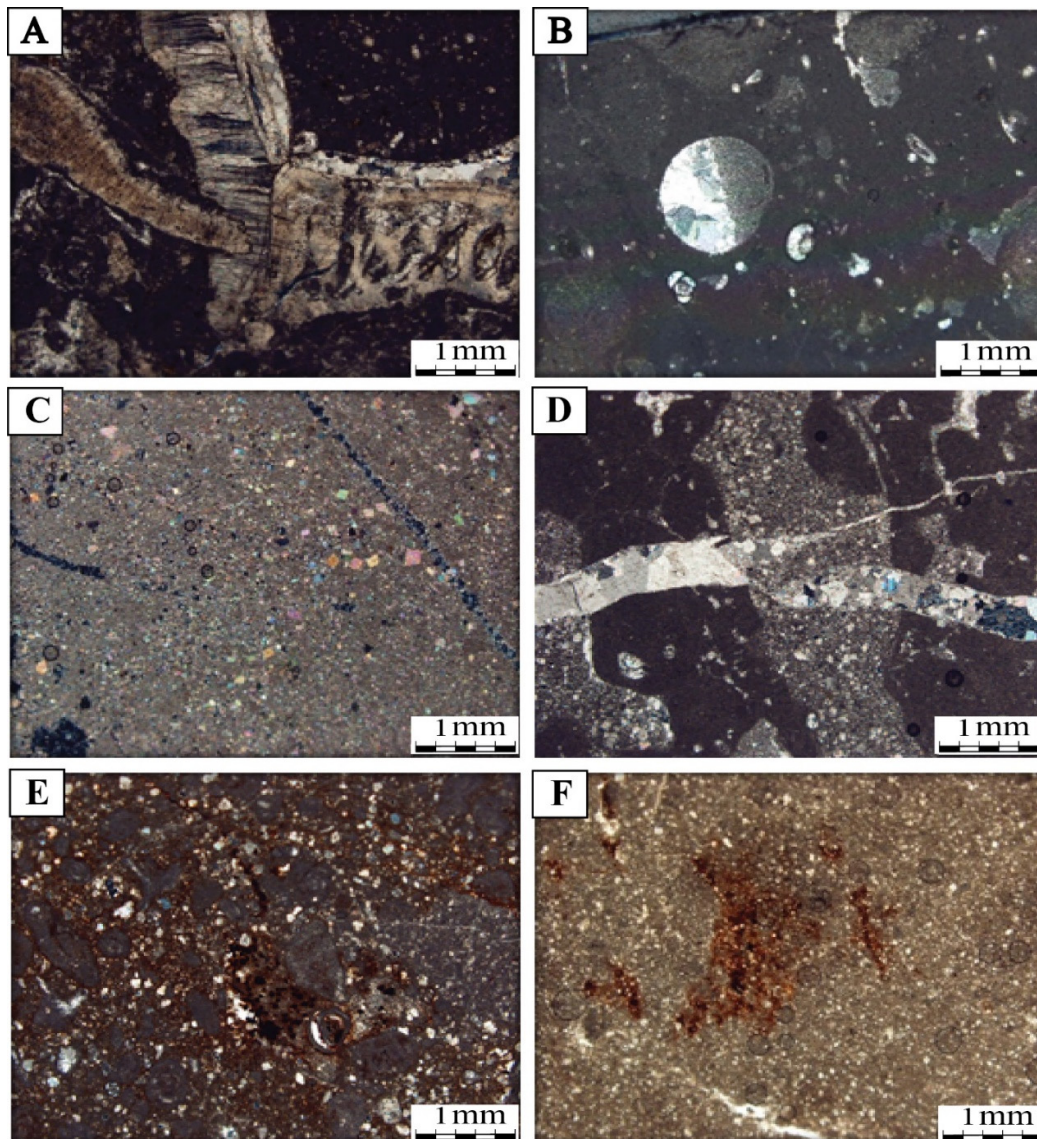


Figure 3 Diagenesis processes identified in the studied section: A. Chemical compaction; B. Geopetal fabric; C. Dolomitization; D. Fracture and filling of veins; E. Iron staining; F. Pyritization

Dolomitization

In this process, limestone or previous sediments are entirely or partially transformed into dolomite because of the replacement of primary calcium carbonate by magnesium carbonate under the influence of magnesium-containing waters. Dolomite can precipitate from waters with different chemical compositions in most stages of diagenesis, i.e. immediately after deposition to deep burial (Hood et al., 2004; Fantle et al., 2020). Dolomitization in the studied thin-sections is the secondary type as coarse and rhomboidal crystals (Fig. 7C). Seemingly, in the studied samples, dolomites are mostly associated with solution seams or stylolites (Enayati-Bidgoli & Navidtalab, 2020).

Fracture and vein filling

In the studied samples, both in the field (Fig. 2E) and in thin-sections (Fig. 7D), calcite-filled fractures are evident. Tectonic activities cause rock fractures during the final stage of diagenesis and when sediments rise (Tucker, 2003). Propagation of fractures is a function of factors such as lithological characteristics, grain size, layer thickness, and stratigraphic features such as facies, sedimentary cycles, and diagenesis (Cooke et al., 2006).

Iron staining

In the studied samples, hematite staining is clearly observed (Fig. 7E). Hematite staining is mostly present in sedimentary facies of tidal flat, lagoon, and shoal environments (Sardar & Tamar-Agha, 2017). The presence of hematite in these samples can be considered a sign of oxic conditions during the deposition of sediments. However, in many cases in the studied section, iron staining is associated with stylolithization.

Pyritization

In the studied sections, pyrite is mainly present between particles in a euhedral form and the space resulting from the dissolution of shells or after the formation of iron-calcite types of cements in a concretionary form (Fig. 7F). Therefore, they are likely due to stylolithization. Pyrite usually precipitates in sediments rich in organic matter. This mineral is included in the initial stage of diagenesis and from the reaction of sulfide (resulting from sulfate reduction) with iron (Taylor & Macquaker, 2000). Fine euhedral pyrite crystals are a common form of pyrite formed during the initial diagenesis stage (Passier et al., 1997). Coleman and Raiswell (1995) believe that euhedral pyrite can be formed during burial. In addition, concretionary pyrites were included due to settling after developing iron-calcite cement, probably in the environments of the final stages of burial.

Discussion

Conceptual depositional model

The depositional model of the basin can be reconstructed by comparing the facies associations with the standard types (e.g. Flügel, 2010). Basically, most of the depositional models are assumed to be rimmed platforms and ramps. In the studied section, the gradual facies transition and the absence of large reef-forming organisms at the edge of the platform may reject the shelf type platform. Therefore, a homoclinal or distally steepened ramp better suits the studied interval (Burchette & Wright, 1992). Although homoclinal and distally steepened ramps

encompass tidal flat, lagoonal, and oolitic and bioclastic barrier shoal facies, they indicate differences in deeper water and basinal deposits (Flügel, 2010). Deeper water facies of homoclinal ramps include fossiliferous wackestones to lime mudstones and marls with diverse biota of open marine. Deeper water facies of distally steepened ramps indicate similar facies but may have breccias and turbidites on the transition of the ramp to basin (Burchette & Wright, 1992; Flügel, 2010). In the studied section, turbidites with grain grading appear on the transition between mid and outer ramp settings and suggest a distally steepened ramp type with a break at the onset of outer ramp (Fig. 8) (Read, 1985; Flügel, 2010).

In ramps, extensive continuous reefal margins are absent (Read, 1985; Pomar et al., 2001). A total of eight sedimentary settings were identified through the facies sequence of the Upper Cretaceous sedimentary rocks according to the energy of the environment, the frequency of constituents, and the skeletal and non-skeletal ingredients. The sub-environments include terrestrial, proximal lagoon, mid lagoon, distal lagoon (rudistic bioherm), shoal complexes, mid ramp, outer ramp, and basin. In these facies, there are mostly winnowed quartz silts. Invasion of terrigenous sands and conglomerates in the shallow edge of the sedimentary environment imprinted the tidal flat. Therefore, facies of this setting could not be distinguished in the studied section.

The rudist buildups facies consists of boundstones with a large amount of in-situ rudists. Rudists build reefal structures mostly throughout lagoon, on the proximal and distal lagoon margins (Burchette & Wright, 1992; Steuber, 1994, 2000, 2002; Flügel, 2010; van Buchem et al., 2011). The lagoon environment includes carbonate facies with mudstone, wackestone, packstone, and grainstone textures. These facies were deposited in different parts of the lagoon depending on the energy level. Lagoon has low energy and limited water circulation. The shoal complex setting includes packstone to grainstone textures. In this setting, with the increase of energy, the micrite content decreases and the sparite calcite increases. Shoal facies associations separate the open marine facies from the lagoon facies, hence, open marine and lagoon organisms are found in these facies. The mid ramp setting includes wackestone to packstone textures, containing a lot of common open marine organisms, and pelagic fauna such as planktic foraminifera. The outer ramp setting consists mostly of mud/wackestone textures with frequent spicules of siliceous sponge that indicate deeper part of the marine. The basin setting is characterized by radiolarian mudstone which are mainly bioturbated. Although previous studies suggested a shallow environment for the upper Cretaceous strata based on nannofossil assemblages in neighboring sections (Bodaghi et al., 2013; Bodaghi & Hadavi, 2014, 2015), our findings suggest a rather deeper depositional environment for these strata. This difference may arise from the location of the study. Our section was selected near the edge of Alborz and Central Iran subdivisions and may represent the deeper parts of the platform.

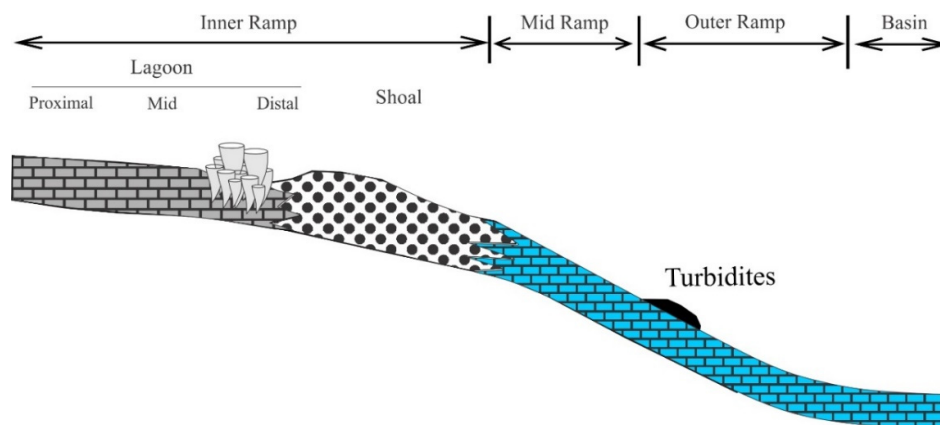


Figure 4 Schematic illustration of the depositional model based on the upper Cretaceous succession in the studied section

Paragenetic sequence

The paragenetic sequence of carbonate rocks can be followed in the initial (eogenesis), intermediate (mesogenesis), and final (telogenesis) stages (Choquette & Pray, 1970). The paragenetic sequence indicates the relative occurrence time of diagenetic processes. The processes include physical and chemical changes during three marine, shallow and deep burial, and uplift stages.

A. Primary diagenesis stage (eogenesis)

The most important diagenetic processes of this stage include boring, micritization, physical compaction, calcite cement precipitation, primary pyritization, and iron-staining (Fig. 9). These processes evidence that the deposits in the studied area have been influenced by marine waters in the first stage. During the early stage of sedimentation in the bottom of the environment under marine phreatic conditions, some allochems were micritized through the biological activity of microorganisms under low energy conditions (Sahraeyan et al., 2013).

B. Middle diagenesis stage (mesogenesis)

The diagenetic processes of this stage occurred during the burial of sediments and increased pressure and temperature, including neomorphism, physical and chemical compaction, dissolution, silicification, dolomitization, blocky calcite cement precipitation, and a part of pyritization (Enayati-Bidgoli & Navidtalab, 2020).

C. Final diagenesis stage (telogenesis)

This stage was formed due to the uplift of limestones. Vein calcite cements, fractures, part of dissolution, and iron staining processes in limestone, mainly occurred through this stage (Enayati-Bidgoli & Navidtalab, 2020).

The diagenetic products indicate that the studied deposits experienced syn- and post-depositional diagenesis via marine diagenetic processes during and a little after sedimentation. These diagenetic products were produced by both marine organisms and waters. Immediately after deposition and during early stage of diagenesis in marine realm, the sediments were affected by meteoric waters that led to dissolution and also cementation of the allochems altered by marine diagenesis. The siliciclastic sediments transported by stream waters denotes pervasive presence of meteoric waters on the nearby territories. Other diagenetic products such as chemical compaction cutting the meteoric diagenetic products notify the occurrence of burial diagenesis after meteoric.

Phase of Diagenesis		Eogenesis		Mesogenesis	Telogenesis
		Marine	Meteoric	Burial	Uplift
Diagenetic Processes	Diagenetic environments				
	Compaction				
	Physical	—————			
	Chemical			—————	
	Micritization	—————			
Cementation	Blocky		—————	
	Isopachos		—————	—————	
	Druzy		—————		
	Geoptal fabric	—————			
	Bioturbation	—————			
	Dolomitization	—————	—————	
	Hematization	—————		—————	
	Fracturing and Filing			—————
	Pyritization	—————		—————	

Figure 5 Paragenetic sequence of the Upper Cretaceous deposits in the studied section

Calcite-filled fractures cut the stylolites and other burial diagenetic products which bear testimony to the diagenetic processes occurring after burial, i.e. telogenesis. Some vein calcite dissolution and vugs also indicate these features as products of telogenesis stage.

Sequence stratigraphy

Combining petrographic and field investigations, vertical and lateral changes in facies, and the position of facies in the depositional environment can lead to interpret sequence stratigraphy (Sarg et al., 1988; Van Wagoner et al., 1988; Haq, 1991; Lehman et al., 2000; Ehrenberg et al., 2007). Sea-level fluctuations during the Cretaceous period in different regions around the world can be inferred from successions deposited in this time-span, which indicate the numerous sea-level rises (Haq, 2014). The paleogeographic location of the studied area was in the Alborz structural zone with severe tectonic activities. Therefore, it is difficult to know the sedimentary history in this area compared to the neighboring regions (Aghanabati, 2009).

Here, terminology and interpretation of sequence stratigraphic scheme follows the simple model Transgressive–Regressive (T–R) of Embry (1993) and Embry (1995). The Cretaceous sedimentary record of the Middle East is divided into three super-sequences (Thamama, Wasia, and Aruma) according to the occurrence of two major unconformities around upper Aptian and upper Turonian (Christian, 1997; Sharland et al., 2001). According to nannofossil studies in neighboring sections, the studied succession is ascribed to upper Campanian–Maastrichtian based on nannofossil zones of CC22 to CC26 (Bodaghi et al., 2013; Bodaghi & Hadavi, 2014, 2015). This interval equals to the top of the upper Cretaceous Megasequence AP9 of the Arabian Plate (Sharland et al., 2001). In the Studied succession, one 3rd-order (Sequence AM: Alborz Maastrichtian) sequence was distinguished based on facies variations and field observations (Fig. 4). The TST (transgressive systems tract) of the sequence AM starts from a sequence boundary occurring on the rudistic massive limestone which forms the HST (highstand systems tract) of the below-laying sequence (Fig. 2A). The TST starts with lagoonal facies and continues to basinal facies to SN90 around 87 m of the section. The top of the rather long interval of outer ramp/ basinal facies is considered as MFS of this sequence which equals MFS (maximum flooding surface) K180 of the middle Maastrichtian (~68 Ma) age of the Arabian Plate. Over this MFS, from SN90, the environment starts shallowing which is reflected in intermittent occurrence of the mid and inner ramp facies that indicate a gradual shallowing upward. Overlaying, the stratigraphic boundary between the studied successions and the Fajan Formation is expressed through a disconformity with sandstones, sandy limestones and iron oxide staining which is considered as sequence boundary type I. This disconformity is in complete concordance with the age and pervasiveness of the upper sequence boundary of AP9 around KPg (~63 Ma). The overlaying formation is conglomeratic Fajan which in parts, its grains size reaches to boulder.

The distinguished sequence AM of the Alborz fits well with the Arabian Plate, and suggests a potential for establishing a framework for the Alborz similar to Zagros and Arabian Plate. However, producing reliable ages and extensive studies are needed to establish a comprehensive sequence stratigraphic framework for the Alborz.

Conclusions

The 120-meter-thick Tuye-Darvar stratigraphic section of the Santonian-Maastrichtian age was studied to reconstruct depositional environment, diagenetic history, and sequence stratigraphy.

Petrographic thin-section inspections led to recognition of a carbonate distally steepened ramp for the studied succession based on the identified microfacies associations of terrestrial, inner ramp (proximal to distal lagoon and shoal), mid ramp, outer ramp, and basin settings.

Detailed examination of diagenetic products in microscopic thin-section studies indicates that these rocks have been affected by various diagenetic processes. During eogenesis in marine environment, micritization, bioturbation, and physical compaction occurred. Through meteoric diagenesis, blocky, drusy, and isopachous types of calcite cements formed. During mesogenesis, physical and chemical compaction, dissolution, silicification, dolomitization, blocky calcite cement precipitation, and a part of pyritization were left as products of burial phase. Finally, in telogenesis, at the uplift stage, vein calcite cements, fractures, partial dissolution, and iron staining processes in limestone were recorded.

Sequence stratigraphic analysis led to identification of one 3rd-order depositional sequence. The maximum flooding surface of this sequence is equivalent to MFS K180 of the middle Maastrichtian (~68 Ma) age of the Arabian Plate. The top sequence boundary of this sequence, which is expressed as a disconformity between the studied succession and the Fajan Formation, correlates with the upper sequence boundary of megasequence AP9 around KPg (~63 Ma).

Acknowledgments

Islamic Azad University Science and Research Branch and Damghan University are thanked for providing facilities for this research. We sincerely thank the two anonymous reviewers for their in-depth revisions and constructive comments.

References

- Aghanabati, A., 2006. Geology of Iran. Geological Survey of Iran, 516 p.
- Alavi, M., 2004. Regional stratigraphy of the Zagros fold-thrust belt of Iran and its proforeland evolution. *American Journal of Science*, 304: 1-20.
- Alavi, M., 2007. Structures of the Zagros fold-thrust belt in Iran. *American Journal of Science*, 307: 1064-1095.
- Bachmann, M., Hirsch, F., 2006. Lower Cretaceous carbonate platform of the eastern Levant (Galilee and the Golan Heights): stratigraphy and second-order sea-level change. *Cretaceous Research*, 27: 487-512.
- Baques, V., Ukar, E., Laubach, S.E., Forstner, S.R., Fall A., 2020. Fracture, dissolution, and cementation events in Ordovician Carbonate Reservoirs, Tarim Basin, NW China. *Geofluids*, 2020: 1-28.
- Bebout, D.G., Budd, D.A., Schatzinger, R.A., 1981. Depositional and diagenetic history of the Sligo and Huston Formations (Lower Cretaceous) in South Texas. *GCAGS Transactions*, No. 109
- Berberian, M., 1976. Contribution to the Seismotectonics of Iran (Part II). Geological Survey of Iran, 39: 518 p.
- Bromley, R.G., 1996. Trace fossils: Biology, Taphonomy and applications Second edition, Capman & Hall, London, 361 p.
- Bodaghi, F., Hadavi, F., 2014. The biostratigraphy of the uppermost calcareous nannofossils of Cretaceous deposit in both Shahdar and Namazgah sections (NE Iran). *Arabian Journal of Geosciences*, 7: 4793-4808.
- Bodaghi, F., Hadavi, F., 2015. Calcareous nannofossils from Late Cretaceous deposits in Mojen section (NE Iran). *Arabian Journal of Geosciences*, 8: 4001-4009.
- Bodaghi, F., Hadavi, F., Rahimi, B., 2013. Calcareous nannofossils biostratigraphy and paleoecology of the last layers related to eastern Alborz Cretaceous deposits in Cheshmeh ghol ghol section. *Paleontology*, 1: 19-36.
- Burchette, T.P., Wright, V.P., 1992. Carbonate ramp depositional systems. *Sedimentary Geology*, 79: 3-57.
- Choquette, P.W., Pray, L.C., 1970. Geologic nomenclature and classification of porosity in sedimentary carbonates. *Bull. Am. Ass. Petrol. Geol*, 54: 207-250.
- Coleman, M., Raiswell, R. 1995. Source of carbonate and origin of zonation in pyritiferous carbonate concretions: evaluation of a dynamic model. *American Journal of Science*, 295: 282-308.

- Cook, M.L., Simo, J.A., Underwood, C.A., Rijken, P., 2006. Mechanical stratigraphic controls on fracture patterns within Carbonates and implications for ground-water flow. *Sedimentary Geology*, 184: 225-239.
- Christian, L., 1997. Cretaceous subsurface geology of the Middle East region. *GeoArabia*, 2: 239-256.
- Dunham, R.J., 1962. Classification of carbonate rocks according to depositional texture (W.E. Ham, Editor), *Classification of Carbonate Rocks*. American Association of Petroleum Geology, Memoir, 1: 108-121.
- Embry, A.F., 1995. TR sequence—the practical genetic unit for stratigraphic analysis, *Proceedings of the Oil and Gas Forum '95*. Geological Survey of Canada, Open File, 187-192.
- Embry, A.F., 1993. Transgressive-regressive (T-R) sequence analysis of the Jurassic succession of the Sverdrup Basin, Canadian Arctic Archipelago. *Canadian Journal of Earth Sciences*, 30: 301-320.
- Embry, A.F., Klován, J.E., 1971. A late Devonian reef tract on northeastern Banks Island, NWT. *Bulletin of Canadian petroleum geology*, 19: 730-781.
- Enayati-Bidgoli, A., Navidtalab, A., 2020. Effects of progressive dolomitization on reservoir evolution: A case from the Permian–Triassic gas reservoirs of the Persian Gulf, offshore Iran. *Marine and Petroleum Geology*, 119: 104480.
- Ehrenberg, S.N., Nadeau P.H., Aqrawi, A.A.M., 2007. A comparison of Khuff and Arab reservoir potential throughout the Middle East. *AAPG Bulletin*, 86: 1709-1732.
- Ehrenberg, S.N., Pickard, N.A.H., Svana, T.A., Oxtoby, N.H., 2002. Cement geochemistry of photozoan carbonate strata (Upper Carboniferous-Lower Permian), Finnmark carbonate platform, Brents Sea. *Journal of Sedimentary Research*, 72: 95-115.
- Flügel, E., 2010. *Microfacies of Carbonate Rocks*, 2 ed. Springer-Verlag Berlin Heidelberg, 976 p.
- Fantle, M.S., Barnes, B.D., Kimberly, V.L., 2020. The Role of Diagenesis in Shaping the Geochemistry of the Marine Carbonate Record. *Annual Review of Earth and Planetary Sciences*, 48: 549-583.
- Folk, R.L., 1980. *Petrology of Sedimentary Rocks*. Hemphill Publishing Co, Austin, Texas, 182 p.
- Gharechelou, S., Amini, A., Bohloli, B., Swennen, R., 2020. Relationship between the sedimentary microfacies and geomechanical behavior of the Asmari Formation carbonates, southwestern Iran. *Marine and Petroleum Geology*, 116: 104306.
- Haq, B. U., 1991. Sequence stratigraphy, sea level change and significance for the deep sea. *Sedimentation, Tectonics and Eustasy: Sea-Level Changes at Active Margins*, 12: 1-39.
- Haq, B. U., 2014. Cretaceous eustasy revisited. *Global and Planetary Change*, 113: 44-58.
- Haywood, A. M., Valdes, P. J., Aze, T., Barlow, N., Burke, A., Dolan, A. M., Von Der Heydt, A., Hill, D. J., Jamieson, S., Otto-Bliesner, B. L., 2019. What can Palaeoclimate Modelling do for you? *Earth Systems and Environment*, 3: 1-18.
- Heimhofer, U., Wucherpfennig, N., Adatte, T., Schouten, S., Schneebeli-Hermann, E., Gardin, S., Keller, G., Kentsch, S., Kujau, A., 2018. Vegetation response to exceptional global warmth during Oceanic Anoxic Event 2. *Nature Communications*, 9: 3832.
- Henehan, M.J., Hull, P.M., Penman, D.E., Rae, J.W., Schmidt, D.N., 2016. Biogeochemical significance of pelagic ecosystem function: an end-Cretaceous case study. *Philosophical Transactions of the Royal Society B: Biological Sciences*, 371: 20150510.
- Henehan, M.J., Ridgwell, A., Thomas, E., Zhang, S., Alegret, L., Schmidt, D.N., Rae, J.W., Witts, J.D., Landman, N.H., Greene, S.E., 2019. Rapid ocean acidification and protracted Earth system recovery followed the end-Cretaceous Chicxulub impact. *Proceedings of the National Academy of Sciences*, 116: 22500-22504.
- Hood, S.D., Nelson C.S. and Kamp P.J.J., 2004. Burial dolomitisation in a non-tropical carbonate petroleum reservoir: the Oligocene Tikorangi Formation, Taranaki Basin, New Zealand: *Sedimentary Geology*, 172: 117-138.
- Hull, P.M., Bornemann, A., Penman, D.E., Henehan, M.J., Norris, R.D., Wilson, P.A., Blum, P., Alegret, L., Batenburg, S.J., Bown, P.R., 2020. On impact and volcanism across the Cretaceous-Paleogene boundary. *Science*, 367: 266-272.
- Jalilian, M., Afsharian Zadeh, A.M., Ghomashi, A., 1992. Kiasar map, Geological map of Iran 1:100000 series. Tehran Naqsheh, Geological Survey of Iran, Tehran, Iran.
- James N. P. and Jones B., 2016. *Origin of Carbonate Sedimentary Rocks*, Department of Earth and Atmospheric Sciences University of Alberta Canada, 464 p.
- Khalifa, M.A., El-Ghar, M.A., Al-Aasm, I., 2014. Linking carbonate cyclicity in platforms to

- depositional and diagenetic overprints: an example from the Lower Eocene Drunka Formation, west of Assiut-Minia stretch, Western Desert, Egypt. *Arabian Journal of Geosciences*, 7: 5159-5170.
- Kalanat, B., Vahidinia, M., Vaziri-Moghaddam, H., Mahmudy-Gharaie, M.H., 2015. A Cenomanian-Turonian drowning unconformity on the eastern part of Kopet-Dagh basin, NE Iran. *Arabian Journal of Geosciences*, 8: 8373-8384.
- Kalanat, B., Vahidinia, M., Vaziri-Moghaddam, H., Mahmudy-Gharaie Mohamad, H., 2016. Planktonic foraminiferal turnover across the Cenomanian – Turonian boundary (OAE2) in the northeast of the Tethys realm, Kopet-Dagh Basin, *Geologica Carpathica*, 451 p.
- Lasemi, Y., Jahani, D., Amin-Rasouli, H., Lasemi, Z., 2012. Ancient carbonate tidalites. In: Davis, R.A., Dalrymple, R.W. (Eds.), *Principles of Tidal Sedimentology*. Springer, Heidelberg, 567-607.
- Leckie, R.M., Bralower, T.J., Cashman, R., 2002. Oceanic anoxic events and plankton evolution: Biotic response to tectonic forcing during the mid-Cretaceous. *Paleoceanography*, 17: 13-11.
- Linzmeier, B.J., Jacobson, A.D., Sageman, B.B., Hurtgen, M.T., Ankney, M.E., Petersen, S.V., Tobin, T.S., Kitch, G.D., Wang, J., 2020. Calcium isotope evidence for environmental variability before and across the Cretaceous-Paleogene mass extinction. *Geology*, 48: 34-38.
- Mehrabi, H., Rahimpour-Bonab, H., Hajikazemi, E., Jamalian, A., 2015. Controls on depositional facies in Upper Cretaceous carbonate reservoirs in the Zagros area and the Persian Gulf, Iran. *Facies*, 61, 23.
- Miall A. D., 2016. *Stratigraphy: A Modern Synthesis*, Springer Verlag, Berlin/ Heidelberg, 454 p.
- Miall, A. D., 2006. *The Geology of Fluvial Deposits: Sedimentary Facies, Basin Analysis and Petroleum Geology*, Springer, New York, NY, USA, 582 p.
- Miall, A.D., 2010, *The Geology of Stratigraphic Sequences (2nd Edition)*: Springer- verlag, 522 p.
- Miller, C.R., James, N.P., Bone, Y., 2012. Prolonged carbonate diagenesis under an evolving late cenozoic climate; Nullarbor Plain, southern Australia. *Sedimentary Geology*, 261: 33-49.
- Morad, S., Ketzer, J.M., De Ros, L.F., 2013. Linking diagenesis to sequence stratigraphy: an integrated tool for understanding and predicting reservoir quality distribution. *Linking Diagenesis to Sequence Stratigraphy. Special Publication of the International Association of Sedimentologists*, 45: 1-36.
- Moghadam, H.S., Stern, R.J., 2021. Subduction initiation causes broad upper plate extension: The Late Cretaceous Iran example. *Lithos*, 398: 106296.
- Moghadam, H.S., Stern, R.J., Griffin, W., Khedr, M., Kirchenbaur, M., Ottley, C., Whattam, S., Kimura, J.-I., Ghorbani, G., Gain, S., 2020. Subduction initiation and back-arc opening north of Neo-Tethys: Evidence from the Late Cretaceous Torbat-e-Heydarieh ophiolite of NE Iran. *GSA Bulletin*, 132: 1083-1105.
- Navidtalab, A., Rahimpour-Bonab, H., Huck, S., Heimhofer, U., 2016. Elemental geochemistry and strontium-isotope stratigraphy of Cenomanian to Santonian neritic carbonates in the Zagros Basin, Iran. *Sedimentary Geology*, 346: 35-48.
- Navidtalab, A., Sarfi, M., Enayati-Bidgoli, A., Yazdi-Moghadam, M., 2020. Syn-depositional continental rifting of the Southeastern Neo-Tethys margin during the Albian–Cenomanian: evidence from stratigraphic correlation. *International Geology Review*, 62: 1698–1723.
- Nascimento, G.S., Eglinton, T.I., Haghypour, N., Albuquerque, A.L., Bahniuk, A., McKenzie, J.A., Vasconcelos, C., 2019. Oceanographic and sedimentological influences on carbonate geochemistry and mineralogy in hypersaline coastal lagoons, Rio de Janeiro state, Brazil. *Limnology and Oceanography*, 6: 2605-2620.
- Okazaki, K., Noda, H., Uehara, S., Shimamoto, T., 2014. Permeability, porosity and pore geometry evolution during compaction of Neogene sedimentary rocks. *Journal of Structural Geology*, 62: 1–12.
- Okubo, J., Lykawka, R., Lucas Verissimo Warren, L.V., Favoreto, J., Dias-Brito, D., 2015. Depositional, diagenetic and stratigraphic aspects of Macaé Group carbonates (Albian): example from an oilfield from Campos Basin. *Brazilian Journal of Geology*, 45: 243-258.
- Passier H.F., Middelburg J.J., de Lange G.J., Bottcher M.E. 1997. Pyrite contents, microtextures, and sulfur isotopes in relation to formation of the youngest eastern Mediterranean sapropel. *Geology*, 25: 519-522.
- Pomar, L., 2001. *Types of Carbonate Platforms: A Genetic Approach*. Wiley, 13: 313-334.
- Purser, B.H., 1978. Early diagenesis and the preservation of porosity in Jurassic limestones. *Journal of Petroleum Geology*, 1: 83-94.

- Piryaei, A., Reijmer, J.J.G., Borgomano, J., van Buchem, F.S.P., 2011. Late cretaceous tectonic and sedimentary evolution of the bandar abbas area, fars region, southern Iran. *Journal of Petroleum Geology*, 34: 157-180.
- Piryaei, A., Reijmer, J.J.G., van Buchem, F.S.P., Yazdi-Moghadam, M., Sadouni, J., Danelian, T., 2010. The influence of Late Cretaceous tectonic processes on sedimentation patterns along the northeastern Arabian plate margin (Fars Province, SW Iran), *Geological Society Special Publication*, 211-251.
- Sahraeyan, M., Bahrami, M., Arzaghi, S., 2013. Facies analysis and depositional environments of the Oligocene Miocene Asmari Formation, Zagros Basin, Iran, southwestern Iran. *Journal of Geoscience Frontiers*, 5: 103-112.
- Sahraeyan, M., Bahrami, M., Hooshmand, M., Ghazi, Sh., & Al- Juboury, A.I., 2013. Sedimentary facies and diagenetic features of the Early Cretaceous Fahliyan Formation in the Zagros Fold- Thrust Belt, Iran. *Journal of African Earth Sciences*, 87: 59-70
- Sardar, H.A., Tamar-Agha, M.Y., 2017. Sedimentology and stratigraphy of Geli Khana Formation (Anisian-Ladinian), a contourite depositional system in the northeastern passive margin of Arabian plate, northern Iraq-Kurdistan region. *Arabian Journal of Geosciences*, 10 (5): 118.
- Sarg, J.F., 1988. Carbonate sequence stratigraphy. In: sea level changes – an integrated approach (Eds C.K. Wilgus, B.S. Hastings, C.G.St.C. Kendall, H.S. Posamentier, C.A. Ross and J.C. Van Wagoner), *SEPM Special Publication*, 42: 155–182.
- Scholle, P.A., Ulmer-Scholle, D.S., 2006. A Color Guide to the Petrography of Carbonate Rocks: Grains, Textures, Porosity, Diagenesis. *American Association of Petroleum Geologists Bulletin*, 459 p.
- Sharland, P.R., D.M. Casey, R.B. Davies, M.D. Simmons, and O.E. Sutcliffe, 2004. Chrono-Sequence stratigraphy of the Arabia plate: *Arabian Plate Sequence Stratigraphy: Geo Arabia*, 9: 16- 34.
- Stocklin, J., 1974. Northern Iran: Alborz Mountains. Mesozoic-Cenozoic orogenic Belt, data for orogenic studies; *Geol. Soc. London*, 4: 213-234
- Scotese, C., 2014. Atlas of Late Cretaceous paleogeographic maps, PALEOMAP atlas for ArcGIS, volume 2, The Cretaceous, Maps 16–22, Mollweide Projection.
- Sharland, P.R., Archer, R., Casey, D.M., Davies, R.B., Hall, S.H., Heward, A.P., Horbury, A.D., Simmons, M.D., 2001. Arabian plate sequence stratigraphy. *GeoArabia*, 2: 1-371.
- Steuber, T., 1994. New rudists (radiolitidae) from the upper cretaceous of boeotia, central greece. *Paläontologische Zeitschrift*, 68: 43-62.
- Steuber, T., 2000. Skeletal growth rates of Upper Cretaceous rudist bivalves: Implications for carbonate production and organism-environment feedbacks, *Geological Society Special Publication*, 21-32.
- Steuber, T., 2002. Plate tectonic control on the evolution of Cretaceous platform-carbonate production. *Geology*, 30: 259-262.
- Taylor K.G., Macquaker, J.H.S., 2000. Early diagenetic pyrite morphology in a mudstone-dominated succession: the Lower Jurassic Cleveland Ironstone Formation, eastern England. *Sedimentary Geology*, 131: 77-86.
- Tierney, J.E., Poulsen, C.J., Montañez, I.P., Bhattacharya, T., Feng, R., Ford, H.L., Hönisch, B., Inglis, G.N., Petersen, S.V., Sagoo, N., 2020. Past climates inform our future. *Science*, 370: 3701.
- Tucker, M.E., 2001. *Sedimentary petrology: an introduction to the origin of sedimentary rocks*, 3rd ed. Wiley-Blackwell, 612 p.
- Tucker, M.E., 2003. *Sedimentary Petrology: Third edition*, Blackwell, Oxford, 260 p.
- Tucker, M.E., Wright, V.P., 1990. *Carbonate sedimentology*. Blackwell, Oxford, 482 p.
- van Buchem, F.S.P., Gaumet, F., Vedrenne, V., Vincent, B., 2006. Middle East Cretaceous Sequence Stratigraphy Study, Part 1: Iran. NIOC and IFP, Iran.
- van Buchem, F.S.P., Simmons, M.D., Droste, H.J., Davies, R.B., 2011. Late Aptian to Turonian stratigraphy of the eastern Arabian Plate - depositional sequences and lithostratigraphic nomenclature. *Petroleum Geoscience*, 17: 211-222.
- Vail, P., Audemard, F., Bowman, S., Eisner, P., 1991. The stratigraphic signatures of tectonics, eustasy and sedimentology-an overview. In: Einsele, G., Ricken, W. and Seilacher, A. (Ed.), *Cycles and Events in stratigraphy*, Berlin, Heidelberg: Springer-Verlag, 659-617.
- Van Wagoner, J.C., Posamentier, H.W., Mitchum, R.M., Vail, P.R., Sarg, J.F., Loutit, T.S. Hardenbol, J., 1988. An Overview of the Fundamentals of Sequence Stratigraphy and Key Definitions. In: Wilgus, C.K., Ross, C.A., Kendall, C.G.St.C., Posamentier, H.W., Van Wagoner, J.C., (Eds): *Sea-*

- Level Changes: An Integrated Approach. SEPM Special Publication, 42: 39-45.
- Vial, P.R., F. Audemard, S. Bowman, P. Einsel, and C. Perez- Crus, 1991. The stratigraphic signatures of tectonics, eustasy and sedimentology- an overview In: Einsel, G., Ricken, W., Seilacher, A., Cycles and events in stratigraphy: Springer- verlag, Berlin Heidelberg New Yourk, 617-659.
- Wu, G., Xie, E., Zhang, Y., Qing, H., Luo, X., Sun, C., 2019. Structural diagenesis in carbonate rocks as identified in fault damage zones in the northern Tarim Basin, NW China. Minerals, 9(6): 1-15.
- Zarza A.M., L.H. Tanner., 2010. Carbonates in Continental Settings Geochemistry Diagenesis an applications, Elsevier, 319 p.



This article is an open-access article distributed under the terms and conditions of the Creative Commons Attribution (CC-BY) license.